An infra-red study of the structure of oriented poly(ethylene terephthalate) fibres

M. Yazdanian and I. M. Ward
Department of Physics, University of Leeds, Leeds, LS2 9JT, UK

and H. Brody
ICI Fibres Division, Hookstone Road, Harrogate, UK
(Received 12 March 1985)

Procedures have been developed for quantitative infra-red spectroscopic measurements on poly(ethylene terephthalate) fibres in conventional yarns. Following computer reconstruction methods already established for films, measurements of molecular orientation and *trans/gauche* conformer content have been carried out for a wide range of fibres produced by different processing routes. The *trans* bands can be separated into load-bearing and non-load-bearing conformations, where the former govern the modulus. It is also shown that a quantitative measure of amorphous orientation can be obtained from the infra-red measurements. While there are similarities between the development of overall molecular orientation and changes in molecular conformation for high wind-up speed yarns and drawn yarns produced from a low wind-up speed yarn, there are also major differences, which confirms previous work showing that these two classes of fibres are basically different in structure. These differences are shown by the relationships between the load-bearing *trans* conformations and the amorphous orientation with the overall orientation.

(Keywords: infra-red; poly(ethylene terephthalate; fibres; modulus; crystallinity)

INTRODUCTION

The infra-red spectrum of poly(ethylene terephthalate) (PET), and the changes which occur in this spectrum on drawing the polymer, have been the subject of many publications[1-8]. A particular point of interest has been the changes in molecular conformation which occur, especially the changes in proportion of *trans* and *gauche* conformation of the glycol residue. Whereas previous quantitative studies have been restricted to thin films[6-8], in this publication quantitative measurements of molecular orientation, conformational content and amorphous orientation are presented for fibres in conventional yarns. Results are presented for fibres spun at very high speeds, drawn fibres using these as precursors, and fibres drawn from fibres of low orientation spun at low speeds. The infra-red spectra have been analysed in terms of a computer reconstruction of the spectrum[8]. This reconstruction procedure enables the identification of more than one absorption to be associated with the same vibration of the *trans* or *gauche* glycol residue but in different local environments. Molecular orientation and changes in molecular conformation are examined in the light of the development of crystallinity, and the increase in Young's modulus during the different processes. Results for amorphous orientation are considered, in relationship to both other structural measurements and the development of increasing modulus.

EXPERIMENTAL

Materials

Fibres. The PET fibres for this investigation were prepared at ICI Fibres, Harrogate using large scale spinning and drawing facilities. The specimens fall into three groups as identified in *Table 1*. The first group was prepared by melt spinning at a fixed extrusion temperature of either 288°C or 294°C followed by winding up at a range of wind-up speeds from 1200 to 5100 m/min. The second group consisted of Group 1 specimens drawn from a hot feed roll at 88°C, followed by a hot plate at 180°C to an extension close to their breaking point. The third group were prepared by the more conventional spinning and drawing route, where a spun fibre is produced by spinning to a comparatively low orientation (at a low wind-up speed of 600 m/min) and then hot drawn similarly to a series of draw ratios.

Films. For the 'internal standard' thickness correction to be described below, a series of film specimens of different thickness was required. These were prepared by uniaxial drawing of thin films from an amorphous PET sheet produced by melt extrusion at 295°C on to a chilled roll.

Infra-red measurements

It was clear from the outset that it would be essential to obtain comparatively high quality infra-red spectra from the fibres in the spun yarns if quantitative information were to be available. Much effort was therefore given to the design and construction of a special filament yarn winding apparatus which converted the yarn bundles into flattened parallel arrays to produce excellent quality grids of fibres.

The filament yarn winding apparatus

A manually operated winding apparatus was specially constructed to untwist a multifilament yarn and wind a

0032-3861/85/121779-12$03.00

Table 1 Details of fibre specimens

Specimen identification	Number of specimens	Extrusion temperature (°C)	Wind-up speed (m/min)	Comments
Group 1	10	294	1200, 1800, 2400, 3600, 4200 and 5100	Undrawn
		288	3000, 3600, 4200 and 4650	Undrawn
Group 2	10	294	1200, 1800, 2400, 3600, 4200 and 5100	Group 1 specimens drawn on a hot plate to near breaking point
		288	3000, 3600, 4200 and 4650	
Group 3	7	294	600	Samples drawn to draw ratios of 1,5 2.0, 2.5, 3.0, 3.5, 4.0 and 4.5

single layer as a parallel grid on a square KBr plate. A schematic diagram of the apparatus is shown in *Figure 1*, and a photograph in *Figure 2*. It can be seen that there are three pairs of rollers A, B and C. The gap between each pair of rollers is successively reduced. The gap between the final pair of rollers C is about $1\frac{1}{2}$ times the fibre diameter so that the ribbon of multifilament yarn which emerges is only a single fibre thick. As the yarn is wound up the twist is advanced to the free end and eliminated. Examination of the parallel grids in a microscope confirmed that these consisted of a closely packed flat ribbon of twist-free parallel filaments. No sign of necking, flattening or damage was observed during subsequent microscope examination.

The filament yarn coming off the last roller C is progressively wound in a single layer on the KBr plate D until the required width of parallel fibres is obtained. The winding unit E which does this was designed to provide an infinitely variable pitch setting so that a parallel grid would be achieved for any weight (decitex) of yarn. The variable pitch was accomplished by changing the arm ratio of a special cam. One end of this cam is fixed in the middle of the rod to which the KBr plate is attached at one end; the other end of the cam engages a threaded rod. These two rods are connected together via identical gear wheels. Hence, when the threaded rod is turned, the other rod also rotates, providing a linear motion.

There are two external dials F and G, one of which varies the arm ratio of the cam and the other moves the rod when the KBr plate is held.

It is necessary to produce a calibration graph of the cam setting (i.e. arbitrary scale) *versus* the measured pitch so as to pre-set to the desired distance equivalent to the width of the untwisted ribbon of filaments coming off the final roller. The latter width is calculated by measuring the fibre diameter in a microscope and multiplying this by the number of filaments present in a given yarn. The range of pitch setting was designed to cover between 150 and 1100 μm to accommodate the decitex of most commercial yarns.

Sample preparation

As described above, the winding operation produces a parallel grid of fibres on a KBr plate. This grid is examined in an ordinary light microscope and filament overlap or gaps between filaments are eliminated manually. A spot of liquid paraffin (Nujol) is then applied to the latter KBr plate; a second KBr plate is used to sandwich this one surface. The two plates are held together by a screw and a nut at two diagonal corners. A Hoffman clip with rubber surfaces is used to hold the filament layers in position whilst the filament layers on the outside are carefully cut away with a sharp razor blade. This procedure leaves a thin parallel layer of fibres immersed in Nujol between the two KBr plates.

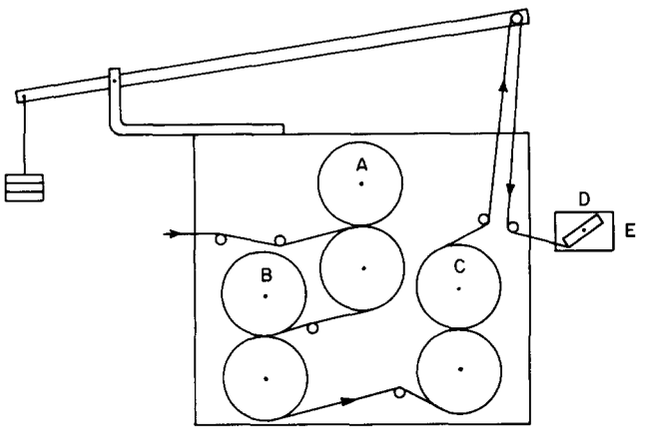

Figure 1 Line diagram of fibre grid winding apparatus

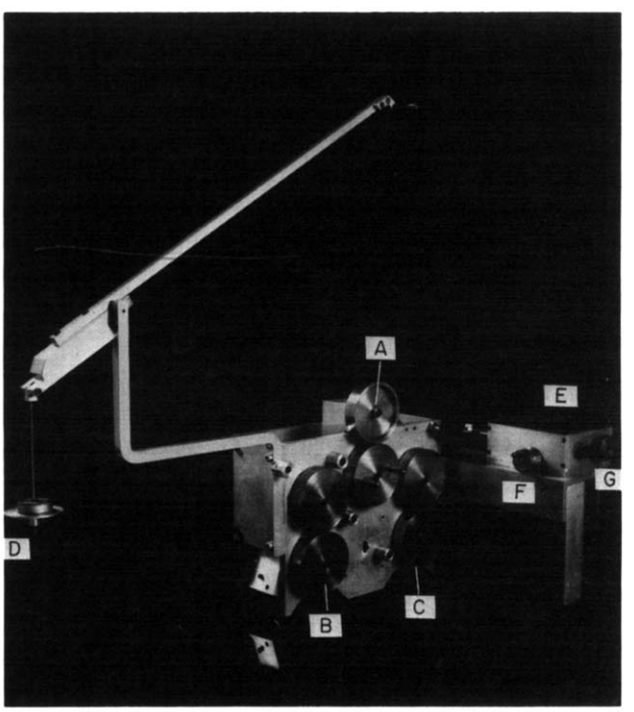

Figure 2 Photograph of fibre grid winding apparatus

Infra-red spectra

The infra-red spectra of the fibre grids were recorded with a Perkin Elmer 580 B ratio recording spectrometer.

Prior to the computer reconstruction of the spectra, the band positions were determined accurately by the calibration of the spectrometer using a standard polystyrene film. The spectrometer was operated in scan mode 4, which gives a resolution of 2.3 cm^{-1}, with a scan speed corresponding to 10 min for the full spectral range 4000 to 180 cm^{-1}, and variable slit width.

The spectral information (i.e. 200 data points at 2 cm^{-1} intervals from 1100–700 cm^{-1}) was directly stored on a floppy disc of the computer attached to the ratio-recording spectrometer and subsequently transferred to the Leeds University Amdahl computer. A file was created for each spectrum, consisting of two sets of data, the absorbances and the corresponding wave-number. Each spectrum so recorded was the numerical average from two runs under identical conditions. From measurements on fibres it was determined that good quality spectra in the region 600–1600 cm^{-1} were only possible where the specimen thickness did not exceed 40 μm. In spite of the additional problems due to possible scattering effects, satisfactory spectra for quantitative analyses could also be obtained for grids of filaments up to 35–40 μm in diameter. The infra-red spectra of fibre grids prepared from the same batch of monofilaments showed reproducibility in absorbances with a range of 4%.

Preliminary measurements on both oriented films and fibre grids showed that the most satisfactory results for polarized radiation were obtained by setting the sample with the fibre axis at $+45°$ to the axis of the entrance slit of the spectrometer. The polarizer, which is the common beam of the spectrometer, was then set at $\pm 45°$ to the axis. Typical spectra are shown in *Figures 3a* and *3b*.

Measurement of refractive indices

The refractive indices of the fibres, n_z and n_x, were measured using an image-splitting Carl Zeiss Interphako interference microscope. Each sample was immersed in a standard refractive index liquid whose index was accurately known and very close to the particular one being measured. The measurements were corrected applying the known temperature corrections for the standard Cargille liquids, and are quoted for a standard temperature of 20°C. The interference technique also provides a value of the specimen thickness, so this was also determined.

Determination of crystallinity

The sample densities were measured with a density gradient column prepared from a mixture of carbon tetrachloride and n-heptane. A rate of fall method was adopted in which the distance travelled by each specimen along the column was recorded as a function of time and the equilibrium position determined from a computer minimization routine. The crystalline fraction x_{cryst} was calculated using the equation

$$x_{cryst} = \frac{d_c(d_0 - d_a)}{d_0(d_c - d_a)}$$

where d_0 is the sample density, d_c = crystalline density, assumed to be 1.455 g cm^{-3}, and d_a = amorphous density, assumed to be 1.335 g cm^{-3}.

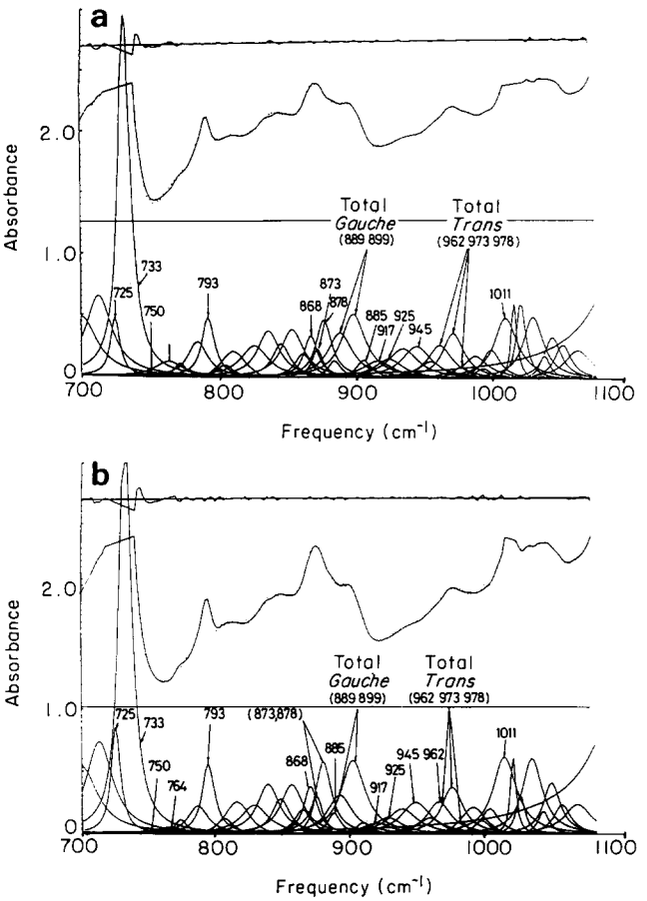

Figure 3 Infra-red spectra of PET fibre (wind up speed 2400/min) between 700 and 1100 cm^{-1}: (a) Polarization direction parallel to draw direction, (b) Polarization direction perpendicular to draw direction

ANALYSIS OF INFRA-RED SPECTRA

Modulus measurements

Modulus measurements were made on an Instron tensile testing machine using a gauge length of 50 cm and a strain rate of 50% min^{-1}. To increase the sensitivity of measurement for initial modulus measurements, the Instron chart speed was increased so that 10 cm of chart were equivalent to 1% strain. The load–strain curves of all the fibres were then found to be perfectly linear up to nearly 1% strain, so that accurate measurements of the initial modulus could be made without drawing tangents to a curve subjectively.

Computer fitting procedures and computational analysis

The procedures adopted for analysing the infra-red spectra followed very closely those described previously for the determination of changes in the spectra observed when PET films were subjected to strain[8]. There is the simplification in the present case that there are no shifts in frequency between different spectra, apart from the 973 cm^{-1} and 978 cm^{-1} bands and to a lesser degree in 889 cm^{-1} and 899 cm^{-1} bands. There is, however, the additional difficulty that the spectra, especially in the parallel polarized radiation condition and for the thicker filaments, show greater absorbances. The steps in the analysis will now be discussed in turn, paying particular attention to new features introduced.

(1) The complete spectrum over the range 700–1080 cm^{-1} was reconstructed. In the present work no direct use will be made of the bands *ca.* 730 cm^{-2} and

1020 cm^{-1} but their wings contribute marginally to the fits for bands *ca.* 795 cm^{-1} and 975 cm^{-1} which will be used for quantitative analysis. The first stage of analysis involved converting the infra-red data to absorbance, and then following a spectrum reconstruction procedure similar to that described previously[8].

(2) In the light of the experience gained in the reconstruction of PET film spectra it was decided to assume from the outset that all the lineshapes (in terms of absorbance) were Lorentzian, including the 725 and 733 cm^{-1} bands which had previously been assumed to be intermediate between Lorentzian and Gaussian. The curve fitting programme fits a set of Lorentzian shaped bands to the measured absorbance spectrum using the method of damped least squares due to Levenberg[9].

Spectra obtained for the Group 1 specimens with wind-up speeds 1200 and 5100 m min^{-1} (see *Table 1*) were used initially to obtain the best fit and to find the positions of new bands which had to be introduced. Subsequently all the specimens in Group 1 were examined before the fitting procedure was finalised. As in the previous case of PET film, both polarization views were fitted simultaneously for all specimens.

(3) The curve fitting procedure commenced by assuming that the positions and line widths of the bands were identical to those found previously for PET film. It soon became apparent, however, that there would have to be significant changes introduced if a good fit was to be obtained. These changes are of two types. In the first place there are some differences in key bands, notably those assigned to *trans* and *gauche* vibrations of the glycol residue. In the previous work a major *trans* band was identified at 973 cm^{-1} and a weak *trans* band at 979 cm^{-1}, both of which shifted to low frequencies under stress. In the present work the major *trans* band at 973 cm^{-1} can again be identified, together with a weaker band at 978 cm^{-1}. It does appear however that there is also a band of medium intensity at 962 cm^{-1} (see *Figure 3*) which was not identified in the film spectra. This band appears to be essential to achieving a good fit and its inclusion as a *trans* band is required to give greatest consistency to the constancy of total *trans* plus *gauche* content (to be discussed in detail later). The fibre spectra are similar to the film spectra in that bands can be identified at 899 cm^{-1}, 889 cm^{-1} and a very weak band at 907 cm^{-1}. The 899 cm^{-1} is the strongest band and is again assigned to a vibration of the *gauche* confirmation. In the previous paper the 907 cm^{-1} was also considered to be a *gauche* band. Our previous work, which covers a wide range of materials, does suggest that again on grounds of maintaining a constant *trans* plus *gauche* content, the 889 cm^{-1} should also be regarded as a *gauche* band. This will be discussed again in greater detail later.

Secondly, it is also necessary to introduce a number of very weak new bands if a good fit is to be obtained. As in the previous work, the existence of such bands in the second derivative spectrum was used as a criterion for their validity. As before, the technique of Savitsky and Golay[10] was followed, and the peak intensities of the most intense bands artificially reduced in magnitude at the computational stage, the second derivative data near such peaks being ignored. Histograms, showing the number of times a peak appears in the second derivative spectra, were used as an indication of the presence of these weak bands.

A careful check was also made in the spectra of model compounds to see if confirmation could be obtained for the existence of such bands in PET. These compounds included cyclic tris(ethylene terephthalate) in its crystallographic A and B forms (C3A and C3B), the cyclic tetra(ethylene terephthalate) (C4), the cyclic penta-(ethylene terephthalate) (C5), the cyclic dimer ethylene terephthalate – diethylene terephthalate (C2A), the cyclic bis(diethylene terephthalate) (C2B), the linear tetramer

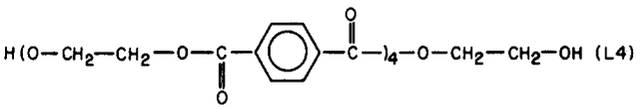

ethylene glycol terephthalate monomer (LM), and ethylene glycol dibenzoate (EGB). The spectra of the last two compounds were reported by Manley and Williams[11]. All the other spectra were obtained from previous work by one of the authors and his colleagues.

Full details of the final fitted spectrum are given in *Table 2*. The peak positions, half widths and other experimental details are provided together with comments indicating the origin of each band where this can be identified. There are only a few weak bands or very weak bands which have no counterpart in the model compounds.

(4) In the previous work on PET films, it was found that as the computer fits were improved, the base-line absorbance corresponded more closely to a linear background, and the final fit for the unstressed film indicated a zero gradient corresponding to 100% transmission. In this present work, the initial attempts at computer fitting included a base-line which was linear but of adjustable slope and also a polynomial base-line shape. It was, however, found that new bands at 778 cm^{-1}, 868 cm^{-1} and 962 cm^{-1} had to be introduced, and that as the fit was improved a zero gradient base-line gave the most consistent results, which is identical to our previous experience for PET films. A further point in the final fitting procedure was the choice of the transmission observed at 920 cm^{-1} as a reference point. It was established by inspection of the spectra for all fibres obtained for both polarization directions that the transmittance was a maximum at 920 cm^{-1} in all cases.

Calculation of orientation averages and concentrations of trans *and* gauche *conformations*

The procedure for obtaining quantitative information from the infra-red spectra follow those described by Cunningham, Davies and Ward[12].

It was assumed that the reflectivity correction is identical to that for film sandwiched between KBr plates with a very thin film of Nujol between each surface. The experimentally observed absorbance A_i for the polarization direction i is then given by

$$A_i = 0.4343\left\{4\pi k_i \frac{y_0}{\lambda} + \frac{2k_i^2}{(n_i + n_{KBr})^2}\right\} \quad (1)$$

where k_i is the true absorbance for polarization direction i, y_0 is the film thickness, λ the infra-red wavelength, and n_i and n_{KBr} the refractive index of the polymer and KBr respectively.

Equation (1) is used to calculate the quantities

$$\phi_i = 4\pi N\langle\alpha_i''\rangle/3 = \frac{6n_i k_i}{(n_i^2+2)^2} \quad (2)$$

Table 2 Peak positions, half width and other details of absorption bands

Band frequency (cm^{-1})	Half width (cm^{-1}) (film)	Fibre/film spectra	Polarization	Intensity	Comments
725	8.2	Fibre and film	σ	vs	Major band in PET
733	10.8	Fibre and film	σ	vs	Krimm assigns to $\delta(CH)_R$
*750	19.8	Fibre	–	vvw	Present in C2A
*764	19.9	Fibre	–	vvw	No band in model compounds
773	10.0	Fibre and film	–	vw	Manley and Williams (775) $\delta(CH)_R$
*778	12.0	Fibre and film	σ	vvw	Present in C3B, C2A, C4
785	17.4	Fibre and film	σ	w	Present in C3A $\delta(CH)_R$ Manley and Williams
793	10.1	Fibre and film	–	m	Major band in PET
*800	9.0	Fibre	–	vvw	Present in C3B, EGB
805	13.5 (8.7)	Fibre and film	σ	vw	Present in C3B, EGB
812	19.2 (10.6)	Fibre and film	–	m	Present in C3A, C2A
819	11.2	Film only	–	vw	Present in C3B, LM
826	14.1 (10.6)	Fibre and film	–	vw	No band in model compounds
837	19.6 (14.6)	Fibre and film	–	w	Present in C3B, C4
846	16.0	Fibre and film	π	m	Major band in PET
854	9.9	Fibre and film	–	w	Present in C3A, C4, C2A, C2B
862	14.2	Fibre and film	σ	w	Present in ethylene glycol
* 868	12.0	Fibre	σ	m	Present in C3A, C5, C2A, C2B
872	9.5	Fibre and film	σ	s	Major band in PET
878	13.8	Fibre and film	σ	s	Major band in PET
* 885	10.9	Fibre	–	w	Present in C3B
889	19.8 (18.8)	Fibre and film	π	w	Present in all cyclic oligomers
899	18.8 (16.7)	Fibre and film	–	m	Major band in PET
907	12.4	Fibre and film	–	vm	Present in EGB
* 913	10.6	Fibre	–	vvw	No band in model compounds
* 917	19.8	Fibre	–	vvw	No band in model compounds
* 925	18.7	Fibre	–	vw	Present in CS
935	21.1	Fibre and film	–	vw	Present in C4, C2A, EGB
* 945	20.5	Fibre	–	m	Present in C5, C2A, C2B
955	18.3 (16.3)	Fibre and film	σ	vw	No band in model compounds
* 962	20.6	Fibre	π	m	Present in C5, L4
973	18.7 (16.7)	Fibre and film	π	s	Major band in PET
978	10.3 (14.9)	Fibre and film	σ	vw	Present in EGB and terephthalic acid
984	19.2 (15.7)	Fibre and film	–	vw	Present in C5, C2A and L4
996	13.8	Fibre and film	σ	vw	Present in C2A and terephthalic acid
*1011	18.6	Fibre	π	s	Present in C3A, C3B
1017	4.7	Fibre and film	π	vs	Major band in PET
1021	8.0	Fibre and film	π	vs	Major band in PET
1031	17.7	Fibre and film	–	w	Present in C3A, C3B
1039	9.3	Fibre and film	π	w	Present in C4, C5, C2A
1045	15.0 (10.0)	Fibre and film	–	w	Major band in PET
1052	15.0 (9.7)	Fibre and film	–	w	Major band in PET

where $\langle \alpha_i'' \rangle$ is the imaginary part of the molecular polarizability and N is Avogadro's number.

Combining equations (1) and (2), ϕ_i is calculated from the measured absorbance A_i at intervals of 2 cm^{-1} over a range of 80 cm^{-1} from each side of the half band width position. The integrated intensity of each band is then taken as the quantity $\bar{\phi}_i = \int_{-\infty}^{\infty} \phi_i(\lambda)\, d\lambda$, which for a Lorentzian lineshape can be approximated to

$$\bar{\phi}_i = \frac{\pi}{2} \phi_i^{peak} \Delta x_{1/2} \tag{3}$$

where ϕ_i^{peak} is the maximum value of ϕ_i and $\Delta x_{1/2}$ is the half-band width. The concentration of any absorbing species (e.g. the *trans* concentration) is then proportional to

$$\phi_0 = (\bar{\phi}_z + 2\bar{\phi}_x)/3 \tag{4}$$

where $\bar{\phi}_z$, $\bar{\phi}_x$ are the values of ϕ_i for the polarization direction parallel and perpendicular to the fibre axis respectively.

Following the previous publication the molecular orientation of a given species is given by

$$\langle P_2(\theta) \rangle P_2(\theta_m) = \frac{\bar{\phi}_z - \bar{\phi}_x}{\bar{\phi}_z + 2\bar{\phi}_x} \tag{5}$$

where $\langle P_2(\theta) \rangle$ is the average value of $(3\cos^2\theta - 1)/2$ where θ is the angle between the axis of the molecular species and the fibre axis, and $P_2(\theta_m) = (3\cos^2\theta_m - 1)/2$ is a constant determined by the angle θ_m which the transition dipole moment of the molecular species (e.g. a *trans* conformer or a benzene ring) makes with the molecular axis of the unit (most conveniently the chain axis).

ANALYSIS OF REFRACTIVE INDEX MEASUREMENTS

We have followed the procedures of previous publications[7,12,13] to calculate the optical orientation function $\langle P_2(\theta)\rangle_{opt}$ from the refractive index measurements. These give

$$\langle P_2(\theta)\rangle_{opt}\frac{\Delta\alpha}{3\alpha_0}=\frac{\phi_z^e-\phi_x^e}{\phi_z^e+2\phi_x^e} \quad (6)$$

where

$$\phi_i^e=\frac{n_i^2-1}{n_i^2+2}$$

n_i is the refractive index, (n_z parallel to fibre axis), (n_x perpendicular to fibre axis), $\Delta\alpha$ is the difference between the electronic polarizabilities of a polymer repeat unit parallel and perpendicular to the chain axis, and $\alpha_0=\frac{1}{3}(\alpha_z+2\alpha_x)$ is the mean polarizability. The quantity $\Delta\alpha/3\alpha_0$ may be estimated from the maximum birefringence of a highly oriented sample, and has been taken as 0.105, following previous work.

RESULTS AND DISCUSSION

Determination of effective thickness

It is clearly not feasible to attempt to estimate the effective thickness of the fibre grid from the fibre diameter. Hence an internal thickness reference band had to be selected. Following previous work[13], the 795 cm^{-1} band was chosen and a calibration graph constructed from the measured spectra of a series of PET films. In this case it is not possible to make the reflectivity correction as equation (1) requires a knowledge of the sample thickness. Instead it was assumed that $A_i \propto y_0$, and hence (A_z+2A_x) can be taken as directly proportional to the film thickness. The calibration graph was then used, together with the measurements of $(A_z+2A_x)_{795\,cm^{-1}}$, to determine the effective thickness of each fibre grid (*Table 3*).

Determination of concentrations of trans *and* gauche *conformers*

As already mentioned, there is inevitably some degree of uncertainty regarding the identification of the minor *trans* and *gauche* bands. It therefore appeared advisable to examine the consequence of alternative assumptions with regard to predictions of total *trans* and *gauche* content. Following previous work, this was done on the basis that the extinction coefficients for all *trans* and *gauche* bands are the same. *Table 4* shows the total integrated intensities $\sum \bar{\phi}_0$ *trans* $+\sum \bar{\phi}_0$ *gauche* where the summation is taken over the various possible *trans* and *gauche* bands. It can be seen that very good consistency is obtained by assuming that there are three *trans* bands at 978, 962 and 973 cm^{-1} and two *gauche* bands at 899 and 889 cm^{-1}.

This conclusion receives further support from the excellent correlations between total *trans* and total *gauche* content and the overall orientation. As shown in *Figure 4*, the total *trans* content increases, and the *gauche* content decreases in a very systematic fashion as the overall orientation increases.

Table 3 Fibre diameter and effective thickness

Sample description (Spinning temperature °C; wind up speed *WUS* (m/min); or draw ratio λ)		Fibre diameter (μm)	Effective thickness (μm)
	WUS		
Undrawn	1200	32.0	41.6
294°C	1800	28.2	41.3
	2400	25.8	40.4
	3600	21.3	38.4
	4200	19.7	36.3
	5100	19.4	35.3
288°C	3000	23.6	39.6
	3600	21.6	38.1
	4200	20.2	36.9
	4650	20.1	35.9
	WUS		
Subsequently drawn	1200	20.8	38.0
294°C	1800	19.6	36.3
	2400	18.8	34.9
	3600	18.0	33.8
	4200	15.9	32.7
	5100	16.6	32.9
288°C	3000	18.8	35.1
	3600	17.9	33.9
	4200	18.3	34.3
	4650	17.1	33.0
	λ		
Drawn specimens from	1.5	36.8	42.8
undrawn feedstock	2.0	26.7	40.7
(600 m/min)	2.5	23.9	39.6
	3.0	20.7	38.0
	3.5	19.6	36.1
	4.0	18.7	34.4
	4.5	17.3	33.1

Determination of molecular orientation functions

It is a very straightforward exercise to determine the orientation average $\langle P_2(\theta)\rangle$ for the benzene ring using the 872 and 878 cm^{-1} bands and for the *trans* and *gauche* conformations using the bands identified as *trans* and *gauche*, respectively and taking the total integrated intensities (e.g. for *trans* adding the contributions from the 962, 973 and 978 cm^{-1} bands). *Figure 5* shows the orientation average for the 872 and 878 cm^{-1} bands plotted *versus* $\langle P_2(\theta)\rangle_{opt}$. It can be seen that there is an excellent correlation, consistent with similar studies of PET films[7,13], and indicating the excellent quantitative nature of these infrared measurements on fibres. In *Figure 6* corresponding results for the *trans* bands are presented. As observed for films the *trans* orientation rises more rapidly than the overall orientation given by $\langle P_2(\theta)\rangle_{opt}$ and thus enables us to estimate θ_m (equation (5) above) as 33°. The quantity $(\bar{\phi}_z-\bar{\phi}_x)/(\bar{\phi}_z+2\phi_x)$ for the *gauche* bands was already very small which is interpreted as indicating that the orientation of the *gauche* conformer is always low, as in previous studies[7,13]. On this basis the overall orientation given by $\langle P_2(\theta)\rangle_{opt}$ relates to a good approximation to the concentration of *trans* conformers x_{trans} and their orientation $\langle P_2(\theta)\rangle_{trans}$ so that

$$\langle P_2(\theta)\rangle_{opt}=x_{trans}\langle P_2(\theta)\rangle_{trans} \quad (7)$$

Figure 7 shows that there is an excellent correlation between birefringence and $x_{trans}\langle P_2(\theta)\rangle_{trans}$, although this diverges from the identity implied by equation (7), especially at low orientation. It can be concluded that the

Table 4 Various internal checks

Sample description (Spinning temperature (°C); wind up speed *WUS* (m/min); or draw ratio λ)		$\langle P_2(\theta)\rangle_{opt}$	$x_{trans}\langle P_2(\theta)\rangle_{i.r.trans}$	% *trans* X_i	% *gauche* Y_i	(X_i+Y_i)
	WUS					
Undrawn	1200	0.018	0.010	21	77	98
294°C	1800	0.069	0.035	24	75	99
	2400	0.123	0.068	26	73	99
	3600	0.234	0.159	32	68	100
	4200	0.302	0.222	35	64	99
	5100	0.419	0.344	43	56	99
288°C	3000	0.179	0.111	28	71	99
	3600	0.251	0.175	34	67	101
	4200	0.349	0.272	39	61	100
	4650	0.392	0.321	41	58	99
	WUS					
Subsequently drawn	1200	0.778	0.748	77	25	102
294°C	1800	0.755	0.735	74	25	99
	2400	0.732	0.720	73	26	99
	3600	0.684	0.678	71	31	102
	4200	0.660	0.641	66	33	99
	5100	0.630	0.635	67	33	100
288°C	3000	0.661	0.671	71	31	102
	3600	0.640	0.671	72	30	102
	4200	0.616	0.657	69	30	99
	4650	0.595	0.644	68	30	98
	λ					
Feedstock 600 m/min	1.5	0.245	0.170	33	66	99
drawn to various draw ratios	2.0	0.365	0.296	41	59	100
	2.5	0.476	0.425	51	51	102
	3.0	0.501	0.447	52	50	102
	3.5	0.572	0.526	57	43	100
	4.0	0.623	0.592	63	38	101
	4.5	0.696	0.661	69	32	101

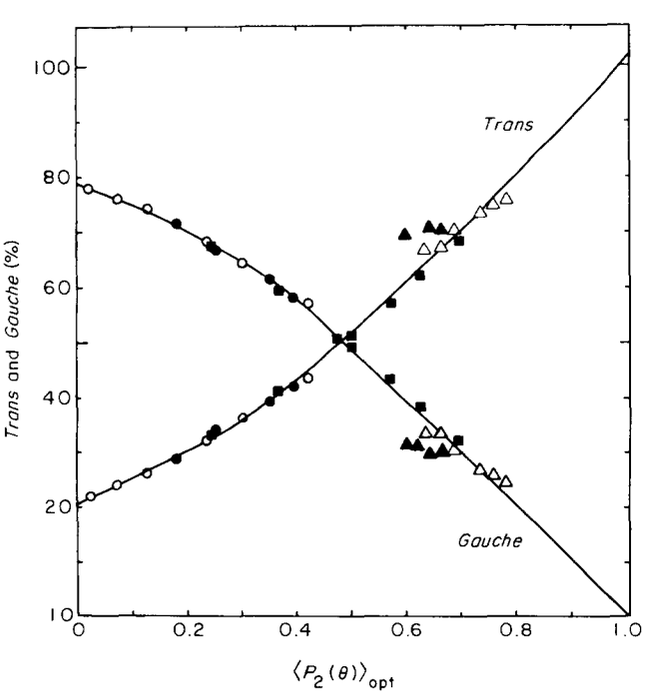

Figure 4 *Trans* and *gauche* content as a function of overall orientation determined by $\langle P_2(\theta)\rangle_{opt}$: (○) 294°C, (●) 288°C, undrawn; (△) 294°C; (▲) 288°C, drawn; (■) drawn from feedstock (600 m/min)

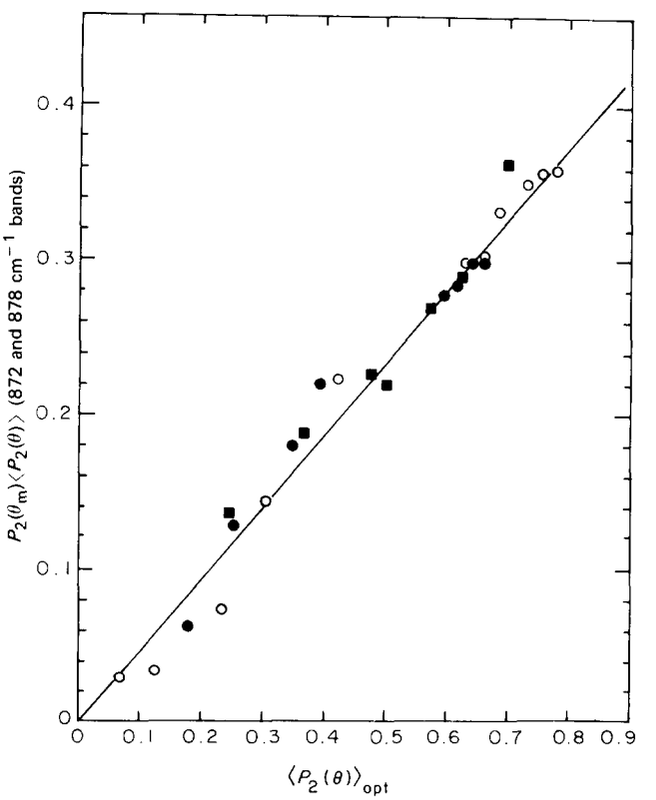

Figure 5 Benzene ring orientation determined from 872 and 878 cm^{-1} bands *versus* optical orientation $\langle P_2(\theta)\rangle_{opt}$ (symbols as in *Figure 4*)

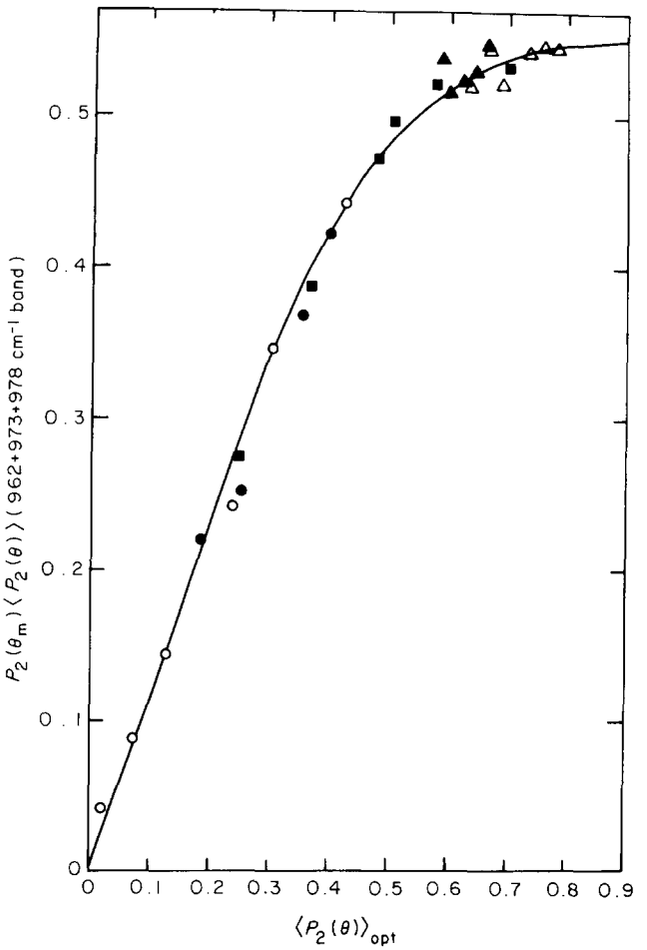

Figure 6 Overall *trans* orientation determined from 962, 973 and 978 cm^{-1} bands *versus* optical orientation $\langle P_2(\theta)\rangle_{opt}$ (symbols as in *Figure 4*)

gauche conformers do make a significant contribution to the overall molecular orientation. This would be expected to be most significant for low values of $\langle P_2(\theta)\rangle_{opt}$ where there is still a substantial concentration of *gauche* conformers as indicated in *Figure 4*. It is interesting to recall at this stage previous results of Padibjo and Ward[13] where equation (7) was examined on the basis of using only the 973 cm^{-1} band as a measure of *trans* content and *trans* orientation. In contrast to the present results it then appeared that there were significant differences between different routes, in that case between single stage and two stage drawn samples, and that equation (7) was only satisfied to a first approximation.

Crystallinity and modulus

Although the overall orientation correlates with orientation of the three *trans* bands, the crystallinity and modulus seems to be mainly dependent on one of these only, the 973 cm^{-1} band, as shown in *Figures 8* and *9*. There is a connection here with the model proposed in ref. 14. Type I crystallization was defined as extension and orientation of 'backbone' molecules which carry the load. It appears that the *trans* conformers thus formed can be identified with the 973 cm^{-1} band. This concept is in excellent agreement with the work of Statton, who showed that it is this band which responds to strain[15].

Type II crystallization was defined as epitaxial crystallization onto this 'backbone', with little change in modulus because this rearrangement of molecules contributes little to load-bearing. These also will be *trans* conformers by definition, since only *trans* conformers can crystallize. It would appear that these must be the other two *trans* bands at 962 and 978 cm^{-1} since they contribute to the overall birefringence as shown in *Figure 7*. Thus it looks as if it is possible to separate the *trans* bands into load-bearing and non load-bearing. This conclusion is reinforced by the plot of total 973 cm^{-1} content against orientation in *Figure 10*. The relationship between the spun and drawn fibres are identical to those relating modulus to birefringence in ref. 14. The close similarity of these two figures is a powerful argument for the connection between modulus and the 973 cm^{-1} band. Further support for modulus relating to the concentration and orientation of the 973 cm^{-1} *trans* band, comes from previous work by Padibjo and Ward[13], where the

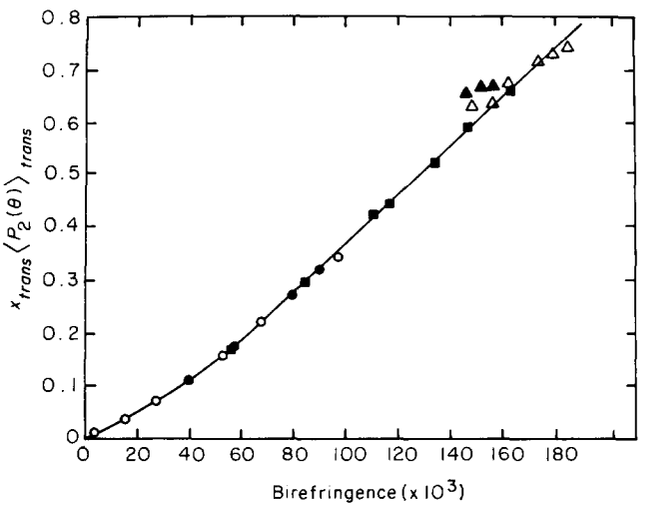

Figure 7 $x_{trans}\langle P_2(\theta)\rangle_{trans}$ *versus* birefringence (symbols as in *Figure 4*)

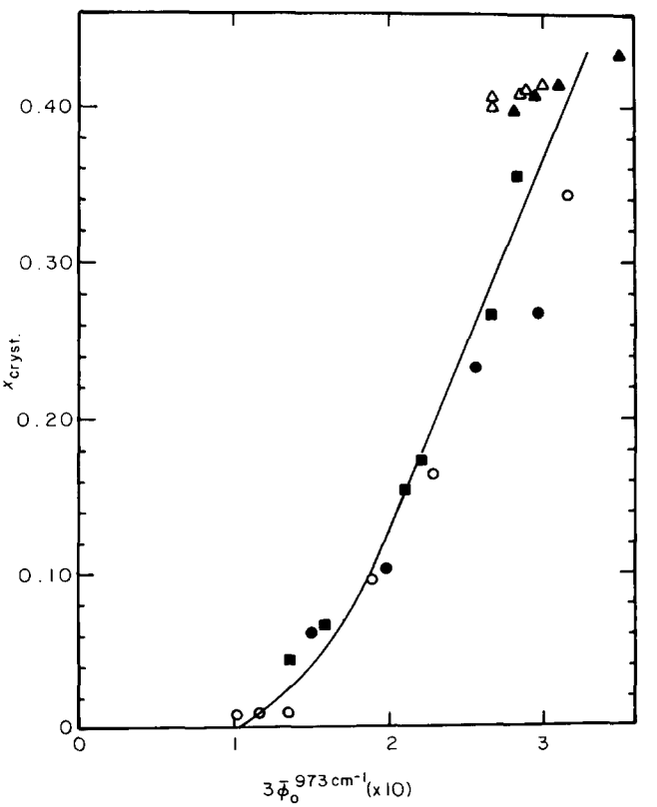

Figure 8 Crystallinity x_{cryst} *versus* concentration of *trans* isomers related to 973 cm^{-1} band only (symbols as in *Figure 4*)

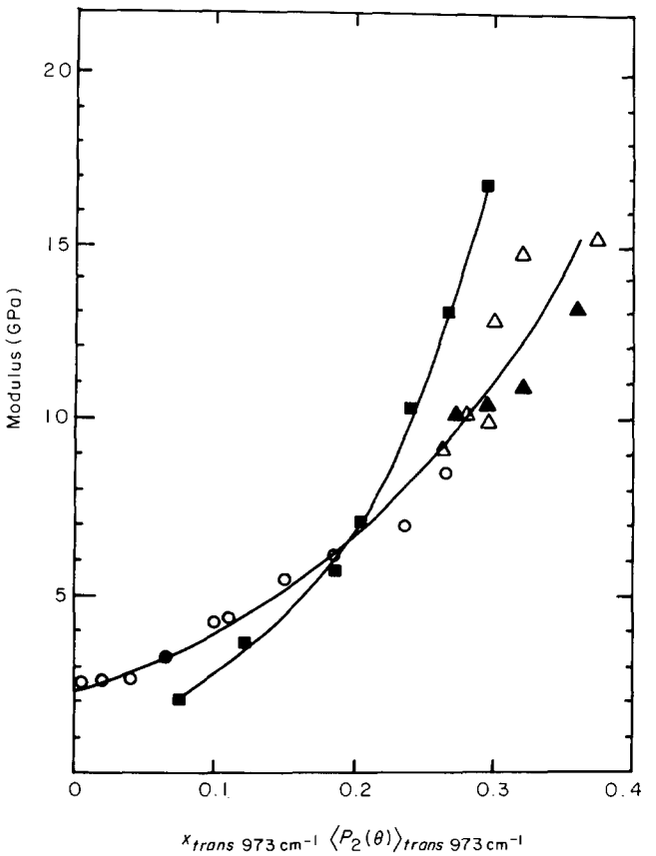

Figure 9 Modulus *versus* $x_{trans}\langle P_2(\theta)\rangle_{trans}$ for 973 cm^{-1} *trans* conformer (symbols as in *Figure 4*)

relationship shown in *Figure 9* was confirmed for one stage and two stage drawn samples. Padibjo and Ward did not find a unique relationship between modulus and birefringence, which can now be seen to be consistent with the present work. The simpler infra-red analysis of Padibjo and Ward ignored the contribution of the 962 and 978 cm^{-1} *trans* bands. Although this is correct for the modulus correlation, the 962 cm^{-1} band in particular makes a substantial contribution to the birefringence, as expressed in equation (7) above.

Of the other two *trans* bands the 962 cm^{-1} makes by far the largest contribution. More information about the 962 cm^{-1} band can be obtained from the plot of crystallinity against the total content of this band in *Figure 11*. It can be seen that the crystallites in the spun fibre must essentially consist of 973 cm^{-1} conformers only, since the 962 cm^{-1} band makes no contribution to the crystallinity. This is consistent with those crystallites being composed of 'backbone' type I crystals only, as postulated in ref. 14. On the other hand, *Figure 11* shows that the 962 cm^{-1} does contribute to the crystallinity in fibres drawn different amounts from the low *WUS* (wind up speed) feedstock. This then is another confirmation of the above hypothesis that it is the 962 cm^{-1} *trans* conformers that subsequently crystallize in an epitaxial fashion.

For fully drawn fibres from feedstock fibres spun at a range of *WUS*, also shown in *Figure 11* the crystallinity is almost constant but the 962 cm^{-1} content has a range of values. This implies that the 962 cm^{-1} band makes no contribution to the crystals in such fibres above a certain level, but is then only reflecting *trans* conformers in the amorphous regions.

In contrast to the 962 cm^{-1} band, there is a good correlation between crystallinity and total 973 cm^{-1} content for both spun and drawn fibres, as shown in *Figure 8*. This again is consistent with 973 cm^{-1} conformers forming the 'backbone' molecules. In spun fibres these conformers must form first as the chains are oriented and *gauche* conformations are transformed into *trans*. They are then the major constituent of the crystalline regions, as pointed out above. The epitaxial contribution of the 962 cm^{-1} occurs with the subsequent

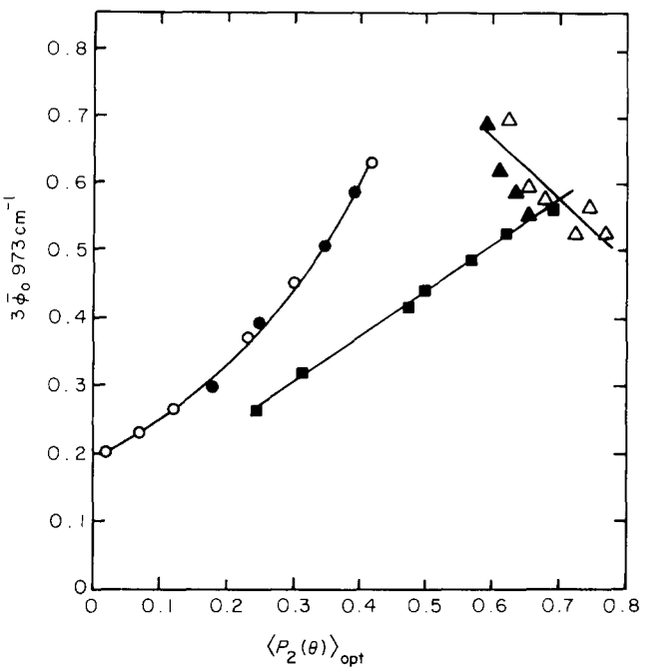

Figure 10 973 cm^{-1} *trans* conformer content *versus* overall orientation determined from $\langle P_2(\theta)\rangle_{opt}$ (symbols as in *Figure 4*)

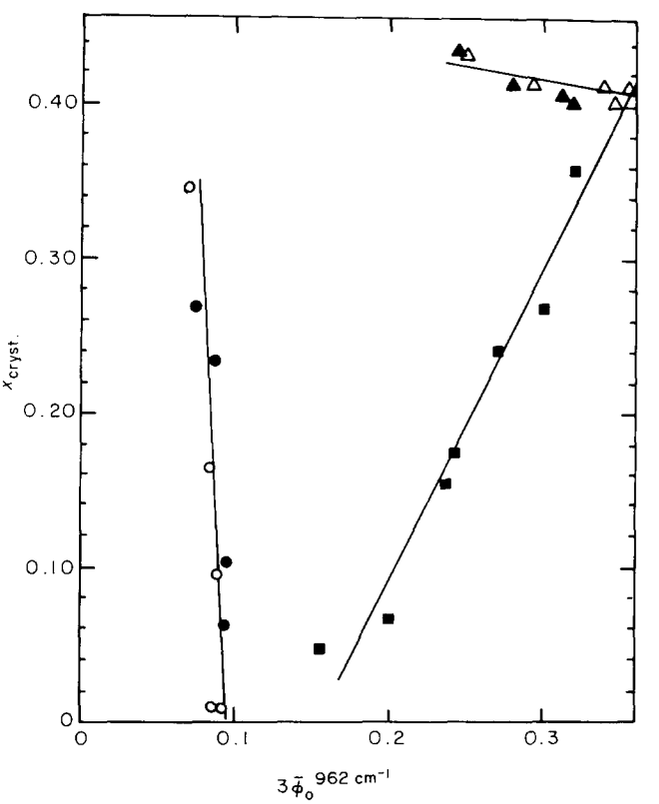

Figure 11 Crystallinity x_{cryst} *versus* 962 cm^{-1} *trans* content (symbols as in *Figure 4*)

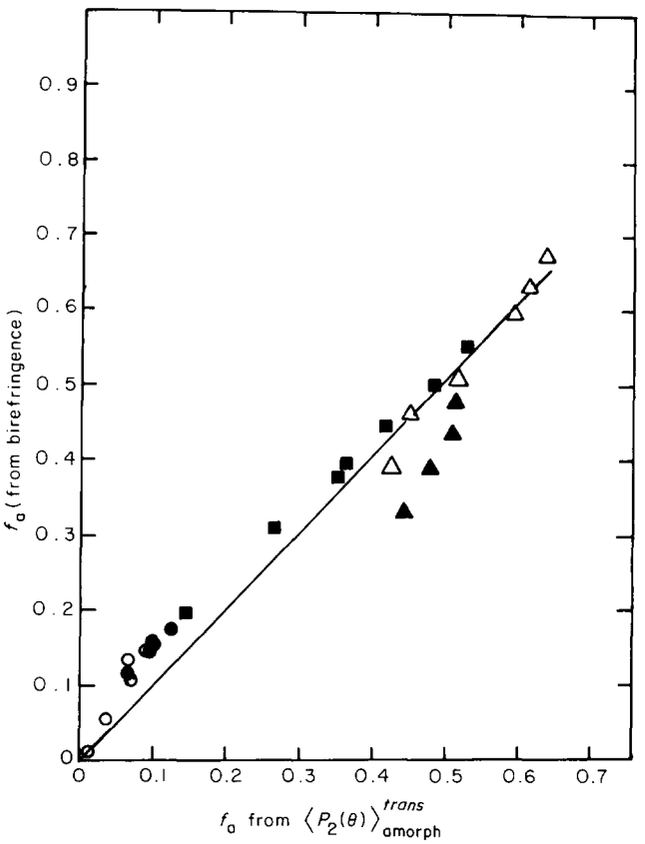

Figure 12 Amorphous orientation f_a determined from birefringence *versus* f_a determined by infra-red spectroscopy (symbols as in *Figure 4*)

heat treatment associated with drawing, and this conformer therefore contributes to the crystallinity of drawn fibres, as shown in *Figure 11*.

It can be seen from *Figure 8* that there is an excellent correlation between the crystallinity and the 973 cm^{-1} *trans* band for both spun and drawn fibres. This relationship is very valuable since it means that subsequent functions derived from partitioning between crystalline and amorphous regions, e.g. the amorphous orientation coefficient f_a, can be derived from i.r. spectra alone without the necessity to determine the crystallinity from a separate density measurement.

Orientation of the non-crystalline regions

Following procedures developed in previous publications[13], an amorphous orientation function f_a can be calculated in two ways. First, by combining birefringence and X-ray diffraction data, we have

$$f_a = \frac{\Delta n - x_{cryst} f_c \, \Delta^\circ n_c}{(1 - x_{cryst}) \, \Delta^\circ n_a} \tag{8}$$

where Δn is the birefringence, $\Delta^\circ n_c$ and $\Delta^\circ n_a$ are the maximum birefringences of the crystalline and amorphous phases respectively, x_{cryst} and $f_c = \langle P_2(\theta)\rangle_{cryst}$ are the proportions and orientation averages for the crystalline regions respectively. In calculating x_{cryst}, corrections were not made for crystal density as in ref. 14 since the fibre species covered a large range (*Table 1*). This would give somewhat higher crystallinities and lower values of f_a for fibres spun at high speed, as compared with ref. 14. f_c was estimated by comparison with previous studies to range from 0.92 to 0.94.

Secondly, on the assumption that $\langle P_2(\theta)\rangle_{gauche} = 0$ we have

$$f_a = \langle P_2(\theta)\rangle_{amor} = \frac{x^{trans}_{amor}}{1 - x_{cryst}} \langle P_2(\theta)\rangle^{trans}_{amor} \tag{9}$$

If both x_{cryst} and x_{trans} are determined, then x^{trans}_{amor} can be estimated. $\langle P_2(\theta)\rangle^{trans}_{amor}$ is then determined from the relationship

$$x^{trans}\langle P_2(\theta)\rangle^{trans} = x_{cryst} f_c + x^{trans}_{amor}\langle P_2(\theta)\rangle^{trans}_{amor} \tag{10}$$

In *Figure 12*, the results of these two methods of obtaining f_a are illustrated. It was assumed that $\Delta^\circ n_c = 0.22$ and $\Delta^\circ n_a = 0.24$[14]. There is a reasonably good correlation, similar but not quite identical to that obtained previously for oriented PET films[13]. The difference between the two methods of obtaining f_a is most marked at low degrees of orientation. This can be attributed to the use of the assumption $\langle P_2(\theta)\rangle_{gauche} = 0$, which clearly does not hold in this region, and hence leads to an underestimate of f_a.

Figure 12 shows that the amorphous orientation function f_a is apparently determined by the *trans* orientation in the amorphous regions only. This is to be expected if the *gauche* is isotropic. However, *Figure 13* shows that for the same overall orientation f_a for all the drawn fibres is much higher at high orientations than that of the spun fibres which levels out. This is another major difference between spun and drawn fibres in addition to those discussed in ref. 14. There is apparently a different balance of amorphous and crystalline orientations in the drawn fibres compared with spun but undrawn. For the same overall orientation f_a is lower and f_c is therefore presumably higher in the spun fibres, although this depends on the crystallinity and the consequent partitioning of the orientations. In ref. 16 it was shown that the measured f_c of fibres spun at high *WUS* approaches unity.

It is concluded therefore that there is a much sharper difference between the crystalline and amorphous regions

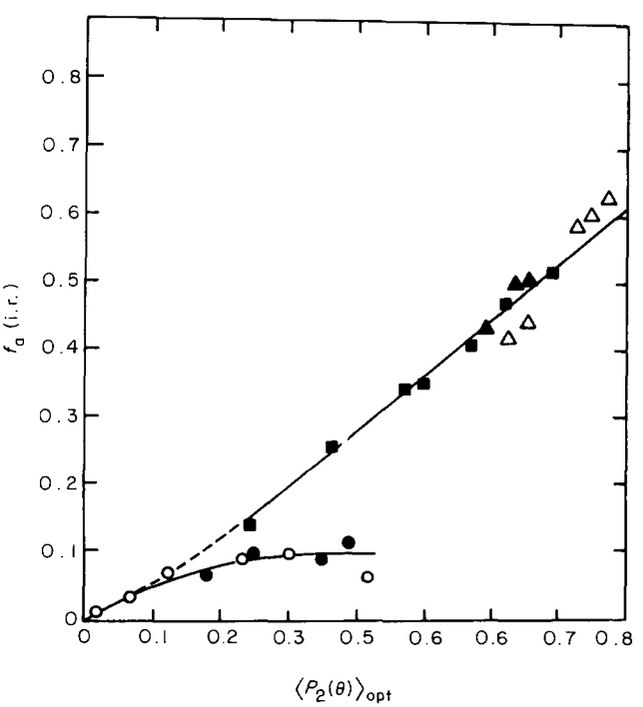

Figure 13 Amorphous orientation f_a *versus* $P_2(\theta)_{opt}$ (symbols as in *Figure 4*)

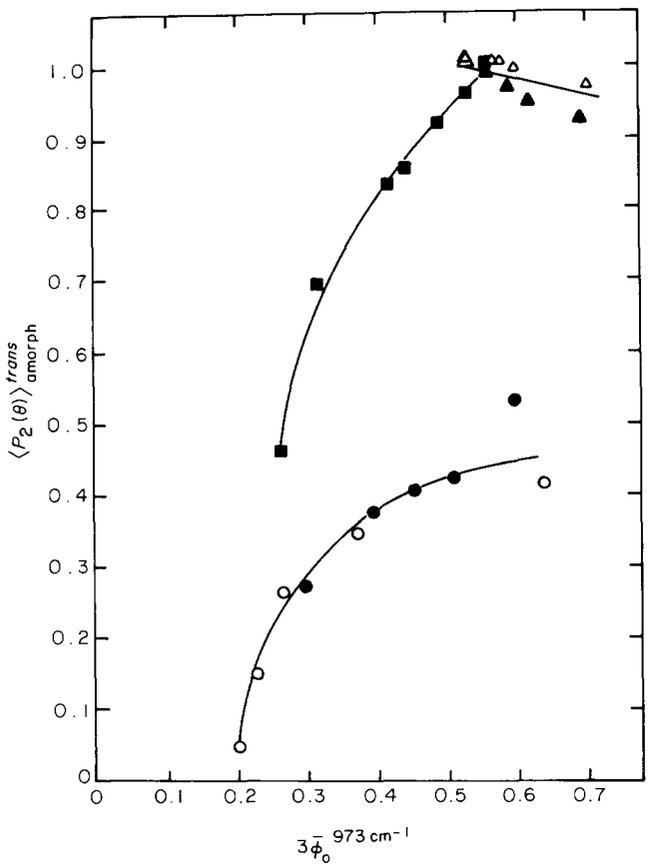

Figure 14 $\langle P_2(\theta)\rangle$ for *trans* amorphous material *versus* 973 cm^{-1} *trans* content (symbols as in *Figure 4*)

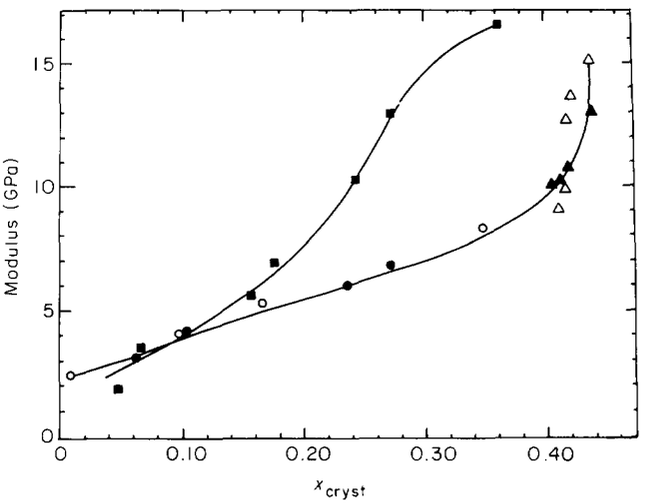

Figure 15 Modulus *versus* crystallinity x_{cryst} for samples prepared by different routes (symbols as in *Figure 4*)

in spun fibres than in drawn. This difference is displayed a different way in *Figure 14*, which shows that for the same 973 cm^{-1} *trans* content the amorphous *trans* are much more oriented in drawn fibres.

A further view of the same situation is shown in *Figure 15*, where the drawn and spun moduli are compared at the same crystallinity, so that the contributions from the amorphous and crystalline regions are normalized, i.e. the total amorphous regions are similar in size. It has been shown above that the modulus correlates with the 973 cm^{-1} *trans* orientation and concentration. Since from *Figure 12* f_a is determined by the amorphous *trans* orientation, this is another demonstration that the drawn amorphous regions are more oriented, via the modulus.

CONCLUSIONS

(1) An infrared spectroscopic method has been devised which enables the accurate determination of molecular orientation and *trans/gauche* conformer content in PET fibres, in conventional yarns.

(2) There is an excellent correlation between total *trans* content (and correspondingly total *gauche* content) and overall molecular orientation, which is closely similar for both high wind-up speed yarns, and drawn yarns produced from a low wind-up speed yarn. The relationship is very similar to that previously observed for drawn films[7,13], where it was concluded that the orientation process related to the stretching of a molecular network, with consequent inevitable correlation between conformational changes and orientation.

(3) The contribution of *gauche* conformers to the overall orientation is comparatively small (except at very low overall orientation), so that the overall orientation relates quantitatively to the proportion of *trans* conformers and their orientation.

(4) There are two major *trans* bands at 973 cm^{-1} and 962 cm^{-1}, with a minor contribution from a *trans* band at 978 cm^{-1}. It seems possible to separate these two major *trans* conformations into load-bearing and non-load-bearing. The most important of these two bands is 973 cm^{-1} since this conformation appears to be the major constituent of the 'backbone' molecules which carry the load and determine the modulus. These particular conformations also predominate in the crystalline regions of spun PET fibres. In contrast, the conformation at 962 cm^{-1} can be identified with the molecules that subsequently crystallize epitaxially onto these backbone molecules on drawing, until the crystallites become saturated when formation of this conformation proceeds in the amorphous regions only.

(5) The orientation of the non-crystalline regions (the so-called amorphous orientation) can be obtained from the infra-red measurements, and the values agree well with those determined from a combination of X-ray diffraction and refractive index measurements. For the same overall orientation the f_a of drawn fibres is much higher, and consequently the f_c of spun fibres must be higher. There is thus a much sharper difference between the orientation of the crystalline and amorphous regions in spun fibres.

(6) The present investigation has also produced a valuable correlation between crystallinity and the 973 cm^{-1} *trans* band concentration.

ACKNOWLEDGEMENTS

This research project was undertaken under the auspices of the ICI Joint Research Scheme, which provided support for Dr M. Yazdanian. We also wish to think Mr. B. Eaden for assistance in the design and construction of the filament winding rig.

REFERENCES

1 Grime, D and Ward, I. M. *Trans Faraday Soc.* 1958, **54**, 959
2 Daniels, W. W. and Kitson, R. E. *J. Polym. Sci.* 1958, **33**, 161
3 Miyake, A. *J. Polym. Sci.* 1959, **38**, 497

4 Liang, C. Y. and Krimm, S. *J. Mol. Spectrosc.* 1959, **3**, 554
5 Farrow, G. and Ward, I. M. *Polymer* 1960, **1**, 330
6 Schmidt, P. G. *J. Polym. Sci.* (A) 1963, **1**, 1271
7 Cunningham, A., Ward, I. M., Willis, H. A. and Zichy, V. *Polymer* 1974, **15**, 749
8 Hutchinson, I. J., Ward, I. M., Willis, H. A. and Zichy, V. *Polymer* 1980, **21**, 55
9 Levenberg, K. *Q. Appl. Math.* 1944, **2**, 164
10 Savitsky, A. and Golay, M. J. E. *Anal. Chem.* 1964, **36**, 1627
11 Manley, T. R. and Williams, D. A. *Polymer* 1969, **10**, 339
12 Cunningham, A., Davies, G. R. and Ward, I. M. *Polymer* 1974, **15**, 743
13 Padibjo, S. R. and Ward, I. M. *Polymer* 1983, **24**, 1103
14 Brody, H. *J. Macromol. Sci.* 1983, **B22**, 407
15 Wool, R. P. and Statton, W. O. *J. Polym. Sci.* 1974, **12**, 1575
16 Heuvel, H. M. and Huisman, R. *J. Appl. Polym. Sci.* 1978, **22**, 2229